Pediatric Radiology (2020) 50:2009–2027
https://doi.org/10.1007/s00247-020-04769-z

FETAL IMAGING

Magnetic resonance imaging of the fetal musculoskeletal system

Nancy A. Chauvin[1] · Teresa Victoria[2] · Asef Khwaja[2] · Hisham Dahmoush[3] · Diego Jaramillo[4]

Received: 4 May 2020 / Revised: 29 May 2020 / Accepted: 1 July 2020 / Published online: 19 November 2020

Abstract

Diagnosing musculoskeletal pathology requires understanding of the normal embryological development. Intrinsic errors of skeletal development are individually rare but are of paramount clinical importance because anomalies can greatly impact patients' lives. An accurate assessment of the fetal musculoskeletal system must be performed to provide optimal genetic counseling as well as to drive therapeutic management. This manuscript reviews the embryology of skeletal development and the appearance of the maturing musculoskeletal system on fetal MRI. In addition, it presents a comprehensive review of musculoskeletal fetal pathology along with postnatal imaging.

Keywords Bone · Development · Fetus · Magnetic resonance imaging · Musculoskeletal · Skeleton

Introduction

Diagnosing fetal musculoskeletal pathology requires understanding normal embryological development. An accurate assessment of the fetal musculoskeletal system must be performed to properly provide optimal genetic counseling and prognostication and to drive therapeutic management [1]. MRI of the fetal musculoskeletal system is considered complementary to US because MRI can confirm abnormalities and provide adjunct information for the fetal surgeon as well as the orthopedic surgeon to aid in surgical planning both prenatally and postnatally [2, 3].

Electronic supplementary material The online version of this article (https://doi.org/10.1007/s00247-020-04769-z) contains supplementary material, which is available to authorized users.

✉ Nancy A. Chauvin
nchauvin@pennstatehealth.psu.edu

[1] Department of Radiology, Hershey Children's Hospital, Penn State Health Milton S. Hershey Medical Center, Penn State College of Medicine, 500 University Drive, Hershey, PA 17033, USA

[2] Department of Radiology, The Children's Hospital of Philadelphia, Perelman School of Medicine at the University of Pennsylvania, Philadelphia, PA, USA

[3] Department of Radiology, Lucile Packard Children's Hospital, Stanford University, Stanford, CA, USA

[4] Department of Radiology, Columbia University Medical Center, New York, NY, USA

Fetal musculoskeletal development

The fetal skeleton develops from primitive mesenchymal cells that are precursors of membranous bone or cartilage. The facial bones, cranium and clavicles develop by intramembranous ossification in which the mesenchymal cells differentiate directly into osteocytes. The skull base, long or tubular bones, pelvis and the vertebral column develop via endochondral ossification in which a cartilaginous model is gradually replaced by bone [4]. Cartilage is identified by 5 weeks of gestation, and by 8 weeks gestation, a complete cartilaginous scaffold is present.

In endochondral ossification, mesenchymal cells differentiate into chondrocytes, which then produce an extracellular matrix. As each long-bone structure lengthens at both ends, the central portion begins to ossify with the help of blood vessels from the surrounding periosteum (Fig. 1) [5]. The long-bone diaphyses enlarge as a result of bone deposition by the periosteum. With advancing gestational age, the border between metaphyseal bone and physis becomes progressively well-defined, with formation of the zone of provisional calcification. There is progressive zonal differentiation of the hyaline cartilage at the ends of the long bones.

The primary physis becomes increasingly distinct from the epiphyseal cartilage. The physis becomes a columnar array of

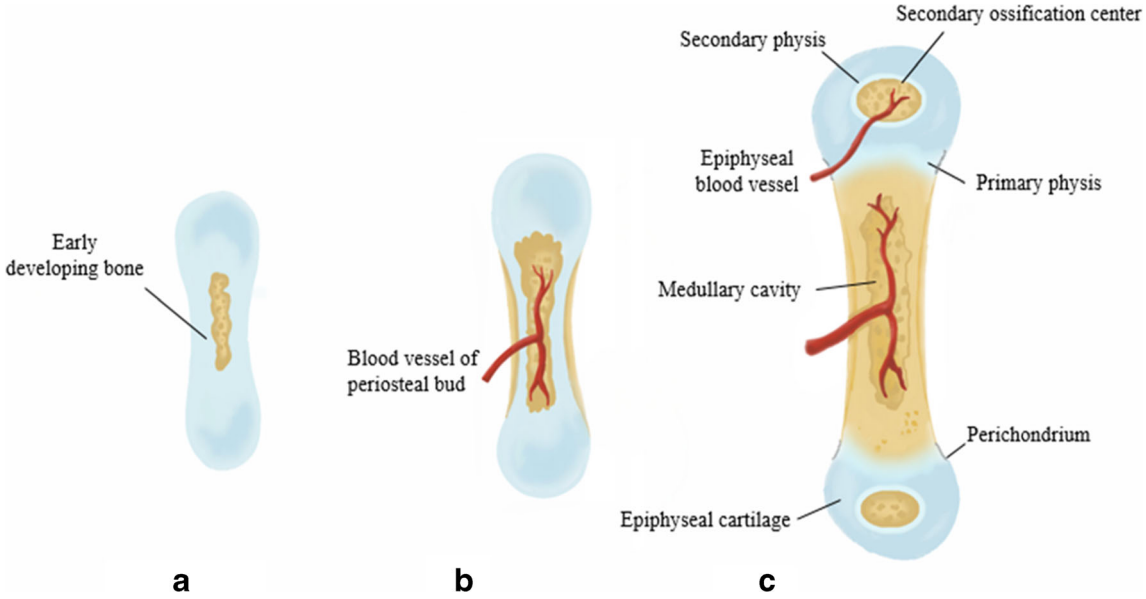

Fig. 1 Schematic of fetal bone development. **a** Cartilage scaffold of a long bone with early ossification centrally. **b** As the long-bone structure lengthens at bone ends, blood vessels from the surrounding periosteum enable growth. **c** With advancing gestational age, the metaphyseal bone is present and the physes become better defined and distinct from the epiphyseal cartilage. Relatively prominent perichondrial structures contribute to physeal development. Secondary ossification centers begin to form in some fetal long bones within the late third trimester

tightly packed chondrocytes responsible for the longitudinal growth of the long bones [6]. In later gestation, the physis is surrounded by perichondrial structures that are relatively prominent. The perichondrium contributes to the organization of physeal chondrocytes into columns of proliferating and hypertrophic cartilage necessary for endochondral ossification. In addition, the perichondrium is responsible for increasing the transverse dimension and providing structural support of the physis. The perichondrium continues to be important in the neonatal and infant skeleton [7]. In the distal femur and proximal and distal tibiae, a secondary center of ossification arises within the epiphyseal cartilage before birth. A secondary physis, surrounding the ossification centers, enables their spherical growth. Gestational age estimations for onset of ossification within the major bones are provided in Fig. 2 [8].

The bulk of the mineralization occurs during the third trimester. In the third-trimester fetus, the diaphyseal cortex is thick, with only a small central medullary cavity that eventually forms the marrow space. Maturation of the fetal skeleton is supported by the placenta as it actively transports calcium, magnesium and phosphorus to appropriately mineralize the skeleton before birth [6]. After birth, bone health is supported by intestinal absorption of minerals.

Normal magnetic resonance appearance of the skeleton during fetal development

The ossified diaphyses appear as hypointense structures and the cartilaginous epiphyses are hyperintense on fluid-sensitive sequences (Fig. 3). In the third trimester, the interface between the bone and the cartilage in the metaphysis is more evident. A well-defined zone of provisional calcification becomes apparent at the interface between metaphyseal bone and physeal cartilage. In the distal femur, the contour of the metaphysis is initially flat and then becomes undulated centrally. This is seen in association with the appearance of the secondary center of ossification. Prominent perichondrial structures, particularly the bone bark, can be readily depicted. As the fetus matures, there is increased differentiation between physeal and epiphyseal cartilage after 32 weeks. Epiphyseal maturation also occurs with the expected contour changes of the cartilage as they progress from rounded structures to their postnatal configuration (Fig. 4). The bone cortex rather than the marrow determines the signal intensity of the bones on fetal MRI. Thus, bones appear as low-intensity structures throughout the body. In late pregnancy, a larger marrow space becomes evident and hematopoietic marrow signal might be depicted [4].

Technical considerations

Imaging at 3 tesla (T) has shown advantage in the depiction of cartilaginous structures and the spine over 1.5-T imaging [9]. Imaging parameters at 1.5 T and 3 T are provided in Table 1. Single-shot fast spin echo (SSFSE), the workhorse sequence of the fetal survey, does not adequately depict the cartilage or perichondrial structures. The sequences outlined next are preferable when imaging the skeletal structures.

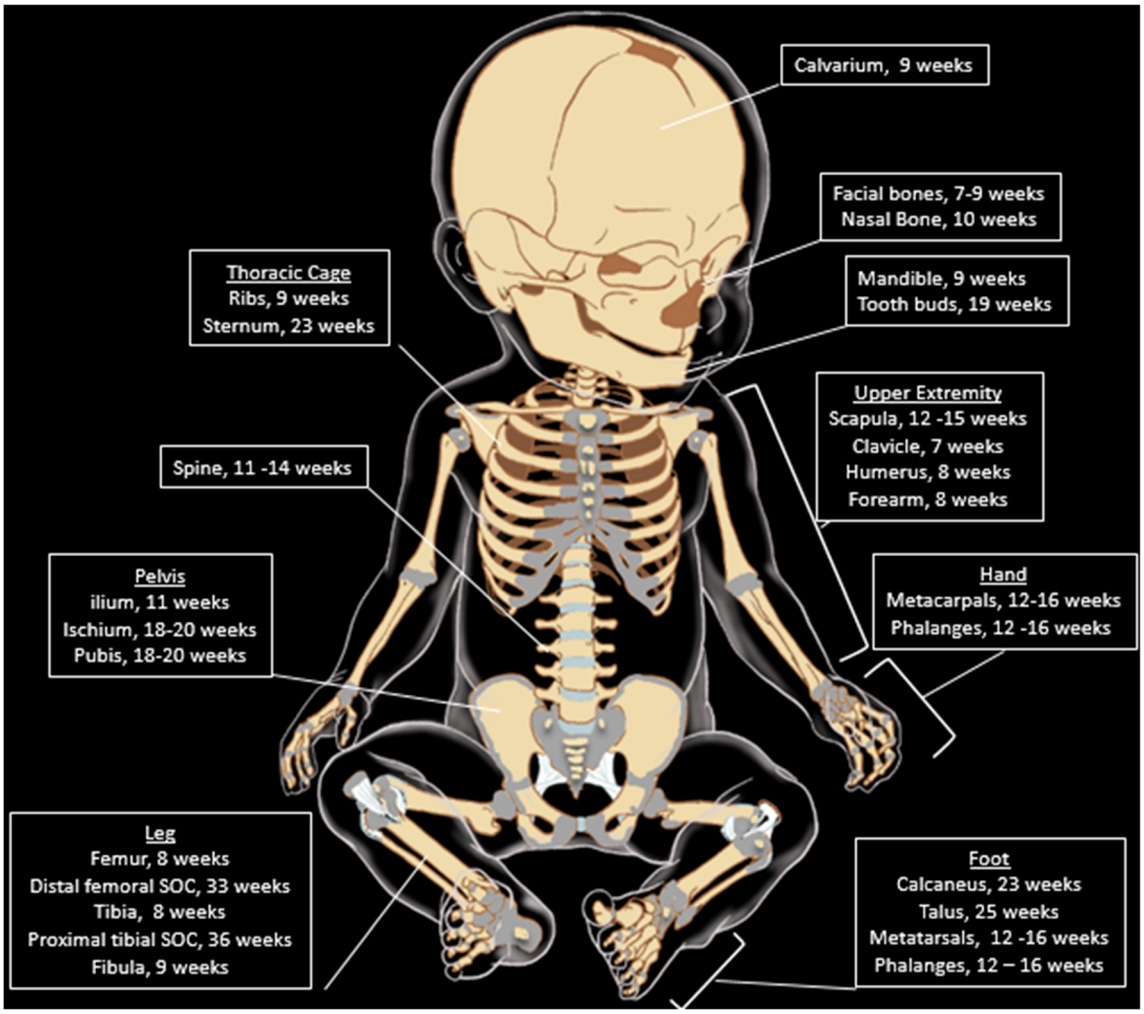

Fig. 2 Gestational age estimations for onset of ossification within the major bones [8]. *SOC* secondary ossification center

T2-weighted steady-state free precession imaging

It is our experience that the best depiction of the fetal skeleton is provided by a T2-weighted two-dimensional steady-state free precession sequence (e.g., true fast imaging with steady precession [TrueFISP]; fast imaging employing steady-state acquisition [FIESTA]; or balanced fast field echo [FFE]). These SSFP sequences provide zonal differentiation of cartilage, excellent depiction of the perichondrial structures, and good definition of bony detail.

Echoplanar imaging

Echoplanar imaging (EPI) provides excellent differentiation between bones and demonstrates osseous structures correlated with gestational age and degree of ossification of the fetal skeleton [1]. The sequence is very fast and thus less susceptible to motion artifacts [1]. EPI is limited by low spatial resolution and low soft-tissue contrast.

Three-dimensional imaging

Three-dimensional (3-D) SSFP sequence provides less contrast between soft tissues, but the 3-D capability can be very useful to depict disorders that are difficult to demonstrate in a single slice [1]. Additionally, the contrast between the fetus and the surrounding amniotic fluid allows surface rendering, which can produce excellent images of the spaces outside the fetus. Thick-slab T2-weighted imaging is acquired in one image and creates a 3-D-like image of the entire fetus that can be manipulated at the workstation (Fig. 5, Online Supplementary Material 1). Because the fetus can be completely visualized on one image, the thick-slab technique can be useful to evaluate limb deformities such as clubfeet or amniotic bands; arthrogryposis; or abnormal proportions as in mesomelic or rhizomelic extremity

Fig. 3 Epiphyses in a 23-week fetus. Sagittal echoplanar MR image of the leg demonstrates hypointense femoral shaft (*bracket*) with hyperintense proximal and distal femoral epiphyses (*arrows*)

shortening present in skeletal dysplasias. The visualization of long bones and extremities on common sequences might be limited by lack of limb continuity in a single image, whereas large field of view in thick-slab T2-weighted imaging allows for complete long-bone visualization. Unlike US, MR is not limited by field of view; therefore, thick-slab sequences can be performed at advanced gestational ages [3].

Dynamic steady-state free precession imaging

Dynamic or cinematic imaging is useful for evaluating movement disorders. Incorporating dynamic SSFP sequences with four to seven images per second allows for real-time demonstration of fetal extremity movement and gross fetal motion. Adding repetitions of this sequence throughout the examination helps overcome temporary variations of malpositioning that could mimic true joint contractures. Any perceived abnormal fetal motion should be evaluated in combination with other musculoskeletal features [3]. Focal limb abnormalities such as clubfeet or hand abnormalities might be more apparent during motion while using cinematic MR (Fig. 6) [1]. Alterations of muscular contour, bulk and signal with increased fat or fluid signal replacing muscle suggest atrophy from neuromuscular disease [10]. The fixed nature of a limb contracture might be visualized as the absence of changes in the extremity's position during the course of the examination. Fetal akinesia, an absence of motion, could indicate a neuromuscular disease in combination with thin muscles [11].

Fetal evaluation

Understanding the embryological development and imaging features of all organ systems of the fetus serves to provide a complete picture to provide optimal counseling for the parents and care for the newborn. Congenital musculoskeletal disorders can occur in isolation or might be associated with more complex anomalies or syndromes [1]. Abnormalities within the musculoskeletal system must be interpreted in the context of other organ anomalies, if present.

Skull and facial bones

Skull

Ossification of the skull occurs via intramembranous ossification from multiple bone centers as they mature throughout pregnancy. The first portions of the skull to

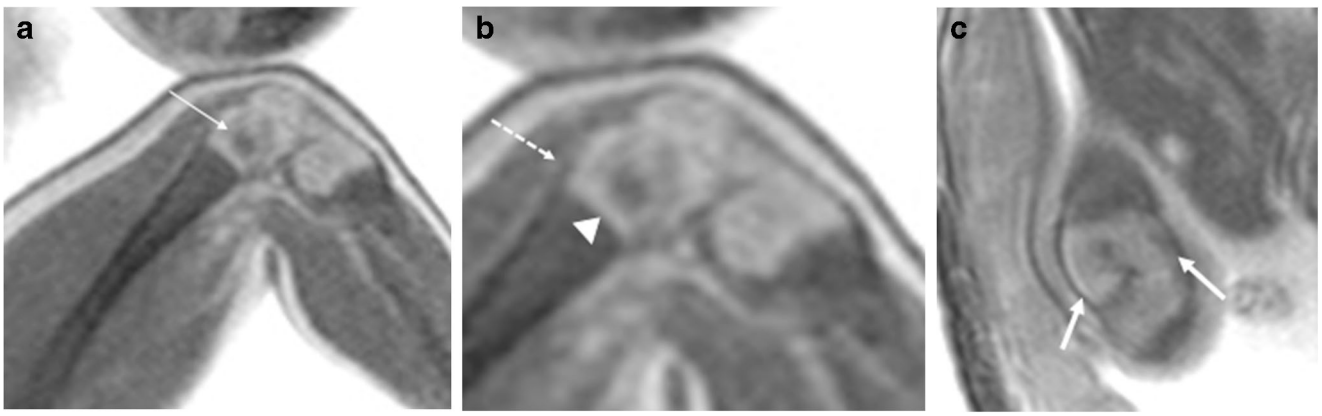

Fig. 4 Epiphyseal maturation in a 34-week female fetus. **a, b** Sagittal T2-weighted steady-state free precession (SSFP) MR images of the fetal leg demonstrate an ossified distal femoral secondary ossification center (*arrow* in **a**). The proximal tibial epiphysis and the patella are entirely cartilaginous. On zoomed image (**b**), perichondrium (*arrow*) surrounds the mildly hyperintense physeal cartilage (*arrowhead*). **c** Coronal T2-weighted SSFP image of the knee shows mature distal femoral epiphyseal contour changes with medial and lateral femoral condyles (*arrows*)

Table 1 Scanner parameters according to field strength and sequence

Sequence	FOV	Matrix	Slice thickness (mm)	Repetition time (ms)	Echo time (ms)	Flip angle (degrees)
1.5 T						
EPI	280×300	256×256	3–10	5,200–6,200	50–60	90
SSTSE	280×300	256×256	3–10	1,100–1,400	75–85	110–180
SSFP 2-D	280×300	256×205	3–10	4	2	45–90
SSFP 3-D	200×200	256×205	3–10	4	2	44–65
SSFP cine	300×300	192×192	3–10	4–275	1–3	37–90
3.0 T						
EPI	280×300	256×256	3–10	4,200–9,000	30–95	90
SSTSE	280×300	320×256	3–10	1,100–1,400	75–100	90–180
SSFP 2-D	280×300	320×256	3–10	4	2	43–70
SSFP 3-D	300×300	256×230	3–10	4	2–3	31–59
SSFP cine	300×300	192×192	3–10	4–400	1–2	36–68

2-D two-dimensional, *3-D* three-dimensional, *EPI* echoplanar imaging, *FOV* field of view, *SSFP* steady-state free precession, *SSTSE* single-shot turbo spin echo

ossify are the basiocciput and orbital roofs, which are typically seen by 9 weeks [8]. These ossification centers are initially scattered in various parts of the individual calvarial bones but rapidly grow and coalesce to form single osseous units. The mesoderm between individual bones forms fibrous tissues, creating the syndesmotic articulations, the sutures. Unlike the frontal and parietal bones, the sphenoid, temporal and occipital bones are formed from several small bones [12]. On MRI, the skull should be evaluated for shape, size and focal skull defects. MRI has the advantage over US of characterizing associated cerebral malformations [11].

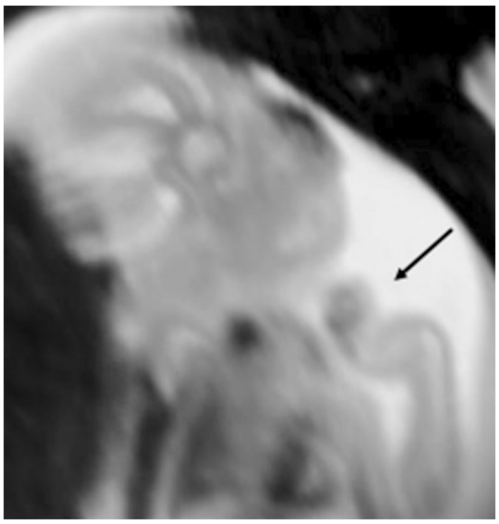

Fig. 5 Thick-slab imaging in a 25-week twin pregnancy — a healthy fetus and a fetus with clubfeet and clenched hands. Representative thick-slab image from a 3-D steady-state free precession MR acquisition shows clenched hand in affected fetus (*arrow*). Post-processing cinematic clip manipulated at the workstation (Online Supplementary Material 1) showed normal fetus followed by affected fetus with clubfeet and clenched hands. (Image and movie courtesy of Dr. Monica Epelman)

Craniosynostosis syndromes

Craniosynostosis is defined as premature closure of the calvarial sutures. The condition can affect one or multiple sutures and is often asymmetrical, resulting in significant skull and facial deformity. Approximately 9% of all cases of craniosynostosis occur as part of a defined syndrome (Table 2), with Apert and Muenke being the most common [13, 14]. Distinguishing isolated single-suture nonsyndromic cases of craniosynostosis from syndromic cases is crucial for appropriate prenatal counseling because syndromic cases are generally more complex and are often associated with developmental delay, central nervous system abnormalities and extremity abnormalities. The process of cranial vault growth is regulated by a variety of genes, including several in the fibroblast growth factor receptor (*FGFR*) family. Genes that most commonly play a role in the pathogenesis of both syndromic and nonsyndromic craniosynostoses are mutations in the *FGFR*, *TWIST* and *EFNB-1* genes [14]. Although sonography has the advantage of being dynamic, it can be hindered by fetal head position or shadowing from the fetal skull [14]. In a review of six cases of craniosynostosis detected by prenatal MRI by Rubio et al. [13], four cases demonstrated developing turricephaly resulting in a characteristic towering contour or "lampshade" sign of the fetal head, which is best seen on coronal images (Fig. 7). The remaining two cases demonstrated a wavy or dysmorphic

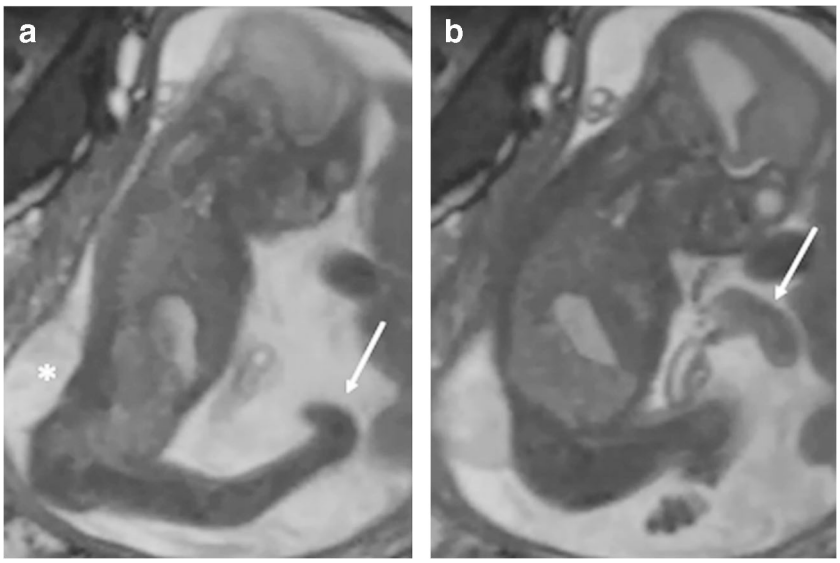

Fig. 6 Cinematic MR in a 24-week male fetus with myelomeningocele and bilateral clubfeet. Select images from dynamic steady-state free precession imaging demonstrate movement of the leg, with the clubfeet becoming readily identifiable. **a** Sagittal image of the leg demonstrates medial orientation of the hindfoot with the foot incompletely visualized (*arrow*). Note myelomeningocele (*asterisk*). **b** Seconds later, the leg is moved and the clubfoot configuration of the foot becomes readily identifiable (*arrow*)

calvarium. A subtle calvarium indentation at the vertex is an early indication of craniosynostosis (Fig. 8).

MRI can be complementary to US to characterize craniofacial relationships and other central nervous system (CNS) and non-CNS findings in the setting of craniosynostosis such as hyper- or hypotelorism, exorbitism from shallow orbits, airway compromise, hand and foot syndactyly, radial ray defect, hernias and heart defects [13, 15, 16]. Hypertelorism is defined as interorbital distance exceeding the diameter of one globe, whereas exorbitism is >50% protrusion of the globe beyond the orbital rim (Fig. 7). Hand syndactyly, such as the typical "mitten deformity" of Apert syndrome (Fig. 7) should be distinguished from clenched fists because clenched fists might raise the concern for an underlying aneuploidy.

Table 2 Features of craniosynostosis syndromes [11, 12]

Syndrome	Common clinical features
Antley–Bixler	Craniosynostosis, midface hypoplasia, elbow synostosis, joint contractures, femoral bowing, dysplastic ears, genitourinary anomalies
Apert	Craniosynostosis, midface hypoplasia, syndactyly of hands or feet, agenesis of the corpus callosum, *consider tracheal cartilaginous sleeve risk*
Baller–Gerold	Craniosynostosis, radial ray hypoplasia or aplasia, anterior or imperforate anus
Beare–Stevenson	Craniosynostosis/cloverleaf, cutis gyrate, anterior anus, genitourinary abnormality, developmental delay, early death
Carpenter	Craniosynostosis, congenital heart disease, umbilical hernia, polysyndactyly of hands or feet, bowed femora or tibiae
Craniofrontonasal	Variable craniosynostosis, often frontal; hypertelorism; bifid nasal lip; longitudinally split nails
Crouzon	Craniosynostosis, midface hypoplasia, anal atresia, milder/variable phenotype, *consider tracheal cartilaginous sleeve risk*
Crouzon with acanthosis nigricans	Craniosynostosis, midface hypoplasia, choanal atresia/stenosis, acanthosis nigricans, narrow sciatic notch, short vertebra (anteroposterior), short and broad metacarpals
Jackson–Weiss	Craniosynostosis, midface hypoplasia, tarsal/metatarsal coalition, broad great toes (normal hands)
Muenke	Craniosynostosis, midface hypoplasia, thimble-shaped middle phalanges, carpal/tarsal fusion, sensorineural hearing loss, cognitive impairment
Pfeiffer	Craniosynostosis; midface hypoplasia; broad thumbs and toes; Type 1, milder; Type 2, cloverleaf, elbow fusion; Type 3, visceral anomalies, without cloverleaf
Saethre–Chotzen	Craniosynostosis, brachydactyly, broad toes, cutaneous syndactyly

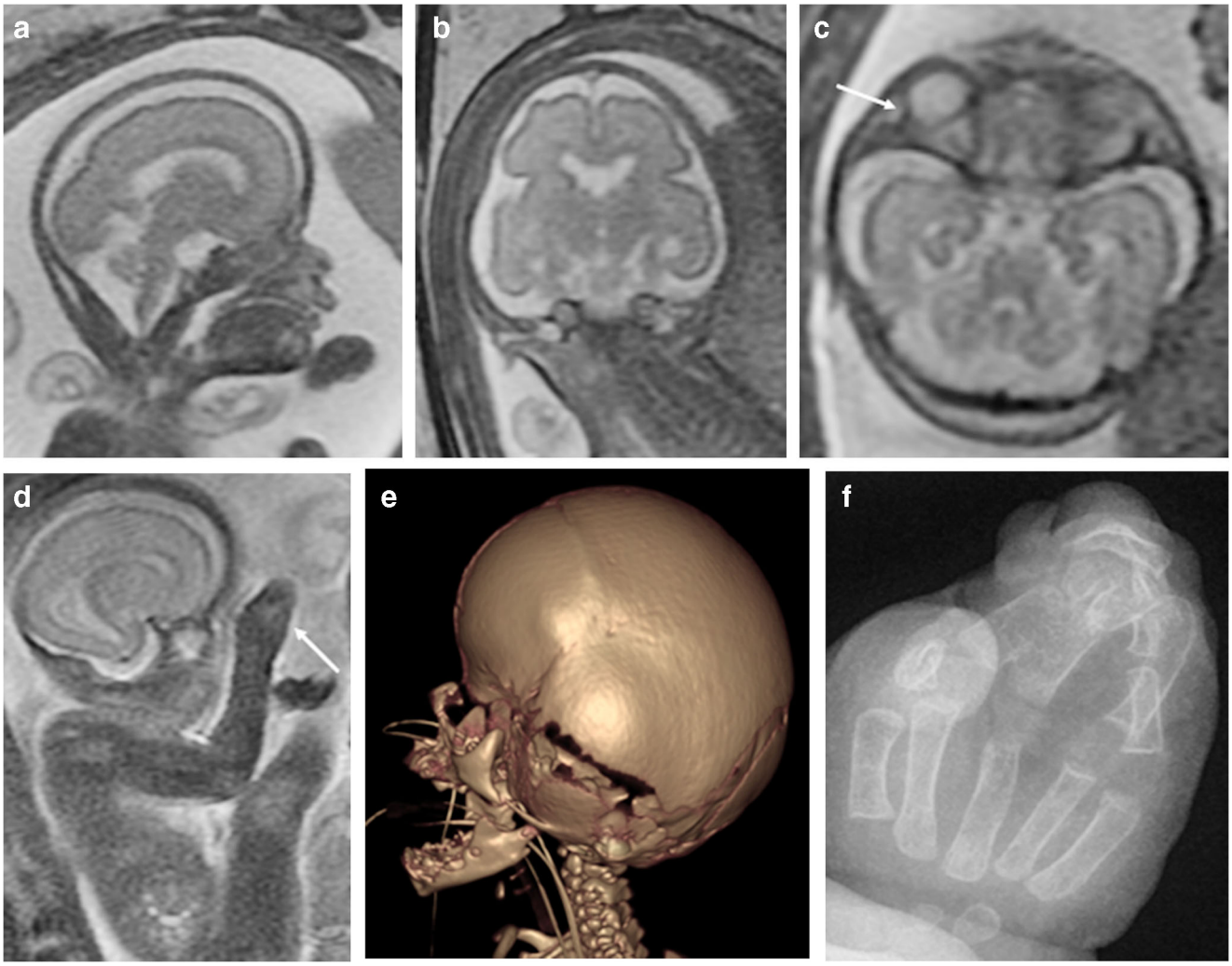

Fig. 7 Apert syndrome in a 26-week male fetus. **a**, **b** Sagittal and coronal T2-weighted steady-state free precession (SSFP) MR images demonstrate brachycephaly and towering calvarial configuration with "lampshade sign" on the coronal image. **c** Axial single-shot fast spin-echo MR image of the head demonstrates exorbitism, with the globe protruding more than 50% beyond the orbital rim (*arrow*), as well as hypertelorism. **d** Sagittal T2-weighted SSFP image shows a clumped appearance of the hand without identifiable digits (*arrow*), in keeping with syndactyly. **e** Postnatal sagittal 3-D reformatted CT image obtained at 13 days of age shows the abnormal calvarial configuration with bicoronal synostosis. **f** Postnatal anteroposterior radiograph of the hand at 16 months of age depicts the "mitten-hand" deformity

Facial bones

The facial bones develop by endochondral ossification from several ossification centers. The maxilla and mandible form by 9 weeks of gestation. Nasal bones are present by 10 weeks. Fetal maxillary dental arch biometry has been explored by MRI with nomograms for the in utero assessment at 18–37 gestational weeks [17]. Reference data for normal mandibular growth on MRI have also been determined [18].

Evaluation of the fetal face is important in cases of skeletal dysplasias, complex malformation and syndromic disorders. The facial profile is typically best depicted on sagittal T2-weighted imaging. Features to look for include glabellar bossing, flattened nasal bridge and micrognathia. The skull base and cranio-cervical junction should be examined with attention to the width and content of the foramen magnum.

Cleft lip and palate

Cleft lip with and without cleft palate is the most common facial malformation. Cleft lip without cleft palate is associated with a favorable prognosis. When the secondary palate is involved, it is a much more complex condition with surgical implications, risk for chronic otitis media, hearing loss, abnormal speech and midface retrusion [19]. While US provides detailed visualization of cleft lips and the anterior palate, the secondary palate is often not well depicted because of acoustic bony shadowing. On T2-

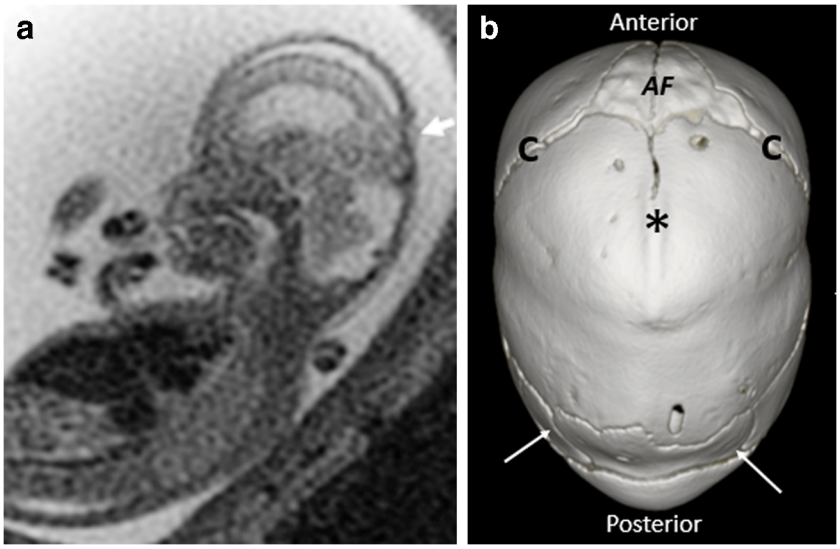

Fig. 8 Gomez–Lopez–Hernandez syndrome and sagittal synostosis in a 19-week female fetus. **a** Sagittal single-shot fast spin-echo MR image of the head demonstrates wavy appearance of the calvarium with subtle calvarial indention at the vertex (*arrow*), an early indication of craniosynostosis, with a tower-shaped calvarial configuration. Multiple brain anomalies were present. **b** Postnatal 3-D reformatted CT scan of the skull shows sagittal synostosis (*asterisk*) and numerous Wormian bones within the posterior aspect of the skull (*arrows*). Clinically, the fetus had focal alopecia and absence of trigeminal nerves on MRI, consistent with Gomez–Lopez–Hernandez syndrome. *AF* anterior fontanelle, *C* coronal sutures

weighted SSFE MRI, cleft lip can be seen as a fluid-filled cleft along the upper lip with hyperintense amniotic fluid extending through the upper lip to the nose and communicating with the nasal passages. Cleft palate is depicted as discontinuous semicircular alveolar ridge contour on axial views with fluid communicating between the oral cavity and nasal cavity (Fig. 9). On coronal imaging, defect of the palate is identified with the nose distorted contralateral to the cleft lip [19]. MRI shows the posterior palate consistently and is superior to US at depicting the secondary palate. However, MRI might be limited in depicting an isolated cleft lip because of partial volume averaging [11].

Micrognathia

Micrognathia or small mandible is thought to result from hypoplasia of the mandibular neural crest cell population. Micrognathia and retrognathia (abnormal mandibular position) typically occur together as a small mandible that is abnormally positioned; this can lead to airway obstruction and respiratory distress shortly after birth [20, 21]. It might be an isolated defect but it is most often associated with other abnormalities. Micrognathia is a feature in more than 300 chromosomal and non-chromosomal conditions and etiologies, including primary mandibular disorders,

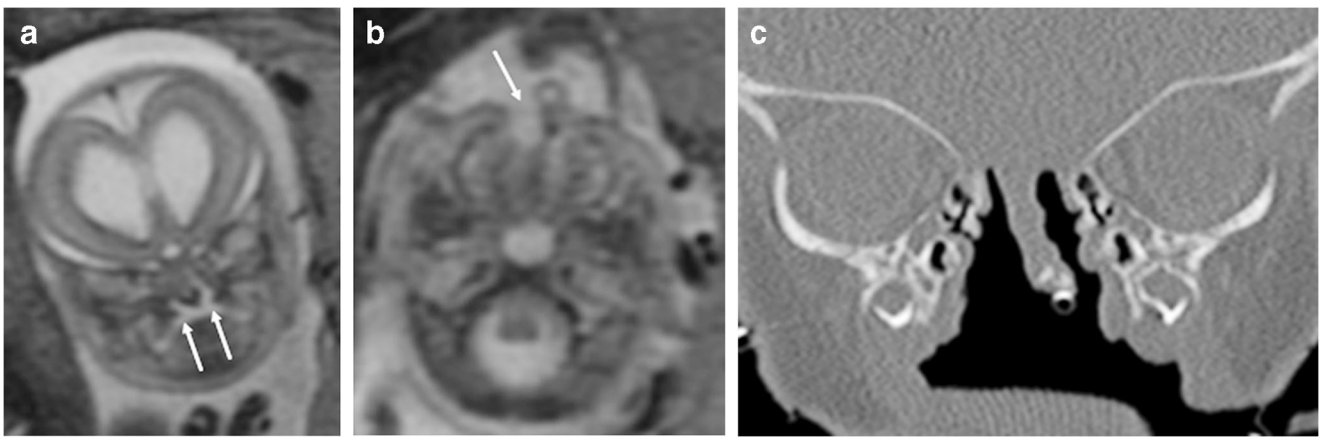

Fig. 9 Cleft lip and palate in a 21-week male fetus. **a**, **b** Coronal and axial single-shot fast spin-echo MR images of the face demonstrate bilateral cleft lip and palate, larger on the right. There is disruption of the alveolar ridge, with fluid communicating between the oral cavity and nasal cavity (*arrows*). **c** Postnatal coronal CT at 11 days of age demonstrates bilateral cleft palate

chromosomal aberrations, syndromes and skeletal/neuromuscular diseases. Common conditions associated with micrognathia are presented in Table 3 [18, 19, 22]. Most cases of micrognathia are related to chromosomal aberration, with an abnormal karyotype reported in 44–66% of cases of fetal micrognathia [22].

MRI has proved to be useful for prenatal diagnosis of microretrognathia, which is of paramount importance because those infants should be delivered in a facility that is able to manage a difficult neonatal airway. While assessment of microretrognathia is largely subjective, measurements can be performed to improve diagnosis. An inferior facial angle is assessed on a mid-sagittal image. The inferior facial angle is defined as the angle formed by a line at the nasal root, which runs orthogonal to the forehead, and a second line from the mentum tip to the anterior border of the upper lip. An inferior facial angle <48–50° reflects micrognathia [18, 20]. The jaw index, another useful measurement, is assessed on axial images. The anterior–posterior diameter of the mandible is measured from the symphysis mentis orthogonally to the level of the posterior borders of the masseter muscles. This is then normalized to the biparietal diameter: (anterior–posterior diameter/biparietal diameter) × 100. A jaw index less than the fifth percentile suggests micrognathia [18]. Of note, the protrusive greater maxillary segment in cleft lip and proclined premaxilla in bilateral cleft might give the appearance of relative micrognathia despite normal mandibular size and position [21].

Pierre Robin sequence is a primary mandibular disorder defined as a clinical triad of micrognathia, glossoptosis and airway obstruction, which is often associated with feeding problems and cleft palate [21]. Micrognathia is the initiating feature of Pierre Robin sequence that leads to glossoptosis and airway obstruction. Glossoptosis is hypothesized to be responsible for the U-shape cleft palate of the secondary palate when present. Many infants with Pierre Robin sequence have other anomalies or a syndrome that prompts prenatal MRI evaluation. Compared to US, MRI provides improved visualization of micrognathia, glossoptosis and cleft palate (Fig. 10) [20].

Spine

Vertebral arch ossification from C1 to the upper lumbar vertebrae is visible at 11–12 weeks of gestation. Vertebral bodies within the thoracic and lumbar spine are ossified by 11–12 weeks as two lateral chondrification centers unite to form the primary ossification center of the vertebral body [8]. The cervical spine vertebral bodies are present by Week 19. Disruption of this process can lead to a segmentation anomaly. While the etiology is unknown, it is postulated that it is caused by a vascular insult supplying that portion of the

Table 3 Common conditions associated with micrognathia [19]

Disorder	Condition
Chromosomal abnormalities	Trisomies 18, 13, 9 and 8
	Turner syndrome
	DiGeorge syndrome
	Deletions of Chromosomes 4 or 5
	Pallister–Killian syndrome
Primary mandibular disorders	Pierre Robin sequence
	Treacher Collins syndrome
	Cerebrocostomandibular syndrome
	Mandibuloacral dysplasia
	Oromandibular-limb syndrome
Skeletal and neuromuscular diseases	Arthrogryposis
	Pena–Shokier syndrome
	Multiple pterygium syndrome
	Osteo-chondrodysplasia
Other syndromic conditions	Meckel–Gruber syndrome
	Noonan syndrome
	Smith–Lemli–Opitz syndrome
	Russell Silver syndrome
	Cornelia de Lange syndrome
	Harlequin syndrome
	Beckwith–Wiedemann syndrome

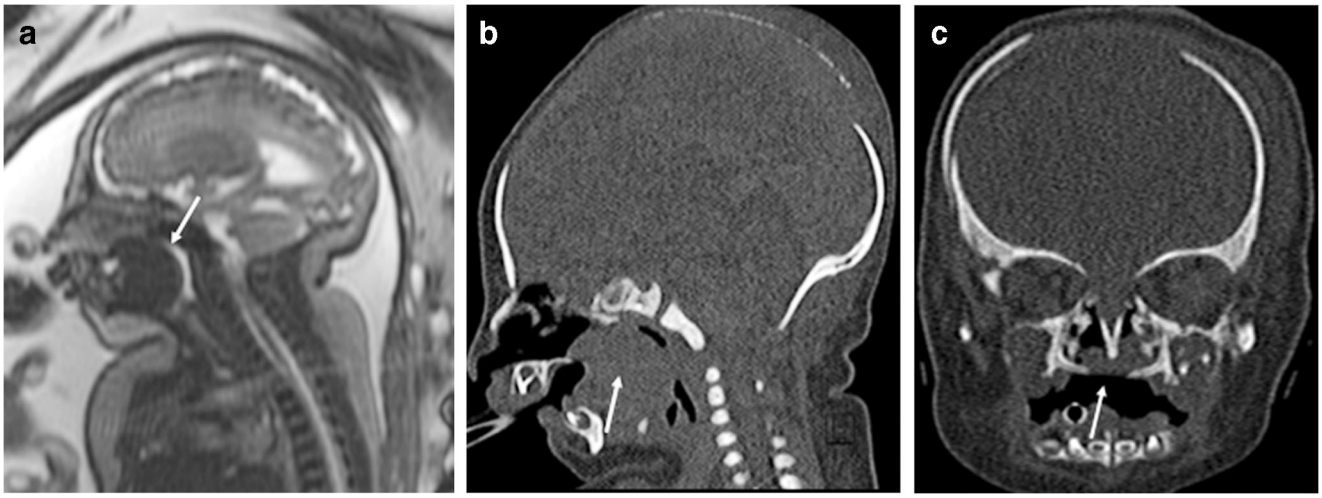

Fig. 10 Pierre Robin sequence in a 35-week male fetus. **a** Sagittal T2-weighted steady-state free precession MR image of the face shows micoretrognathia with glossoptosis and superior extension of the tongue through a secondary palate defect (*arrow*). Inferior facial angle was 44°. **b**, **c** Sagittal (**b**) and coronal (**c**) CT images of the head in bone windows obtained at 1 day of age demonstrate glossoptosis causing airway obstruction (*arrow*) in this intubated boy, who had respiratory distress after birth. Note U-shape cleft of the secondary palate (*arrow*)

vertebral column. Anomalies are broadly classified into two categories: failure of formation and failure of segmentation. Failure of formation includes hemivertebrae and wedge vertebrae, whereas failure of segmentation leads to block vertebrae, unilateral bar vertebrae and atlanto-occipital fusion. These fetuses can present with scoliosis or kyphoscoliosis (Fig. 11). Vertebral anomalies can occur in multiple areas throughout the spine and might be associated with abnormalities in the extremities and other organ systems (cardiac, genitourinary, gastrointestinal and pulmonary) [23]. Platyspondyly might also be depicted on MRI [24]. MRI of the fetal spine is a valuable adjunct to US and often superior to US for assessing suspected spinal malformations, and MRI has the advantage of better depiction of associated CNS and non-CNS anomalies [25]. Spinal dysraphism encompasses a diverse group of spinal anomalies with associated CNS anomalies that can be optimally evaluated on MRI; however, it is beyond the scope of this paper and is addressed in another paper included in this symposium.

Caudal regression syndrome or lumbosacral agenesis is an anomaly of the caudal cell mass/filum terminale and is strongly associated with maternal hyperglycemia. Structurally, fetuses have varying degrees of coccygeal, sacral and lumbar agenesis, with the anomaly progressing caudally to cranial and

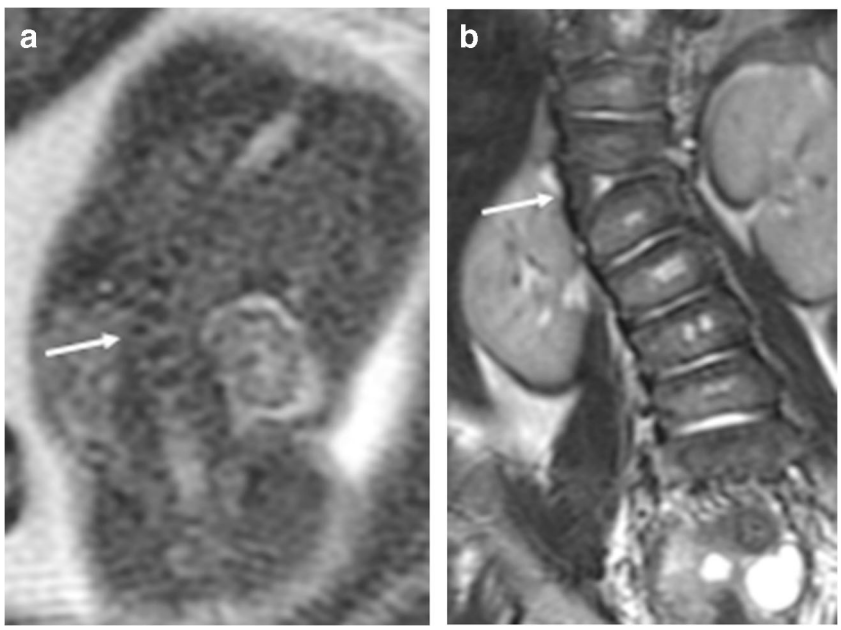

Fig. 11 Scoliosis caused by hemivertebrae in a 21-week female fetus. **a** Coronal single-shot fast spin-echo MR image of the spine shows dextroconvex scoliosis of the thoracolumbar spine caused by hemivertebrae in the upper lumbar region (*arrow*). Additional vertebral anomalies were seen cephalad. **b** Postnatal coronal T2-weighted MR image in the girl at 6 months old demonstrates the hemivertebrae at L1 (*arrow*)

manifesting as sacral agenesis or dysgenesis to sirenomelia (fusion of the lower limbs) [23]. Caudal regression syndrome is divided into two types: in Type 1, the conus medullaris is high and ends abruptly; in Type 2, the spinal cord is tethered and the conus medullaris is low-lying (Fig. 12). Caudal regression syndrome can be found in association with other anomalies such as omphalocele, bladder exstrophy, imperforate anus and spinal defects (OEIS complex); vertebral, anal, cardiac anomalies, tracheoesophageal fistula, renal and limb malformations, hydrocephalus (VACTERL-H); and sacral agenesis, anal atresia and presacral teratoma, dermoid/epidermoid cyst or meningocele (Currarino triad) [25].

Thoracic cage

The rib primordium is present at 5 weeks of development, and rib ossification begins at 9 weeks. During the first trimester, the ribs increase in length and bend toward the sternal anlagen. The first seven "true ribs" connect to the sternum via costal cartilage by Day 45. The lower five "false ribs" do not articulate with the sternum. The sternal primordium begins as a pair of lateral mesenchymal condensations or sternal bars at 6.5 weeks of development. Fusion of the sternal bars occurs at 9–10 weeks, with ossification of the sternum occurring at approximately 23 weeks [8, 26]. Clavicles begin to ossify at 7 weeks and the scapulae by 12–15 weeks.

Evaluation of the thoracic cage should include assessing overall size because a hypoplastic thorax occurs in many skeletal dysplasias such as thanatophoric dysplasia, achondrogenesis, hypophosphatasia, campomelic dysplasia, chondroectodermal dysplasia, osteogenesis imperfecta and short-rib polydactyly, among others. A small thorax can lead to pulmonary hypoplasia, which is a main cause of death in many lethal skeletal dysplasias (discussed later in this manuscript) [27]. The shape should be evaluated, noting rib size and configuration. Rib fusion anomalies in the setting of vertebral anomalies and a foreshortened spine might be indicative of spondylothoracic dysostosis. The presence of the clavicles and scapula should also be noted because deficiency could be indicative of cleido-cranio dysostosis or campomelic dysplasia, respectively [27]. It should be noted that MRI provides limited assessment of complex thoracic and spine anomalies (Fig. 13). In complex skeletal anomalies, ultra-low-dose fetal CT might be considered to improve prenatal counseling and optimize perinatal management [28].

Extremities

Long-bone evaluation is an integral component of the fetal survey because an abnormality could indicate an osteochondrodysplasia or chromosomal anomaly. Complete limb evaluation includes assessing extent of ossification as well as evaluating for long-bone length and the presence of fractures, bowing, polydactyly, syndactyly and limb contracture. Ultrasound is the method of choice for measuring long bones, and femoral measurements are a standard part of the mid-trimester US scan and help confirm gestational age [5]. Femoral or humeral length measurements lower than the 5th percentile or two standard deviations below the mean in the second trimester suggest the presence of a generalized skeletal disorder [1]. MRI can be used to confirm limb abnormalities detected on US and provides additional findings in certain cases.

Ultrasound studies have shown that the presence and size of secondary ossification centers can also be used as a marker

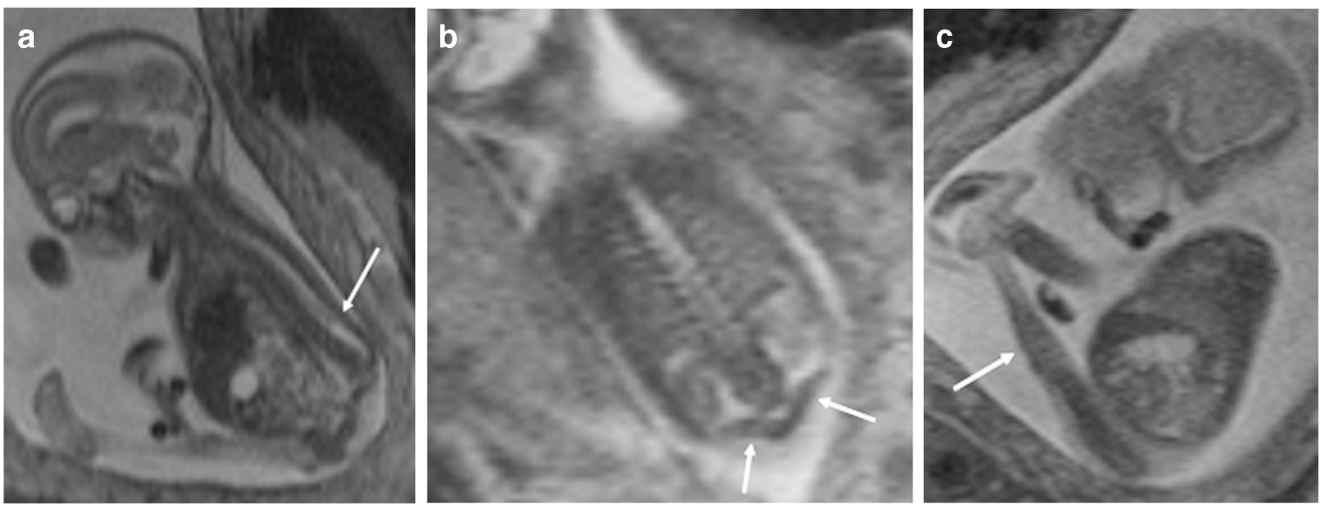

Fig. 12 Caudal regression syndrome in a 20-week fetus. **a** Sagittal single-shot fast spin-echo (SSFSE) MR image of the spine demonstrates abrupt termination of spinal cord (*arrow*). **b** T2-weighted steady-state free precession MRI coronal to the spine shows opposed iliac wings (*arrows*) with absent sacrum. **c** Sagittal SSFSE image shows the knee in extension (*arrow*), evident throughout the study, with decreased muscle bulk

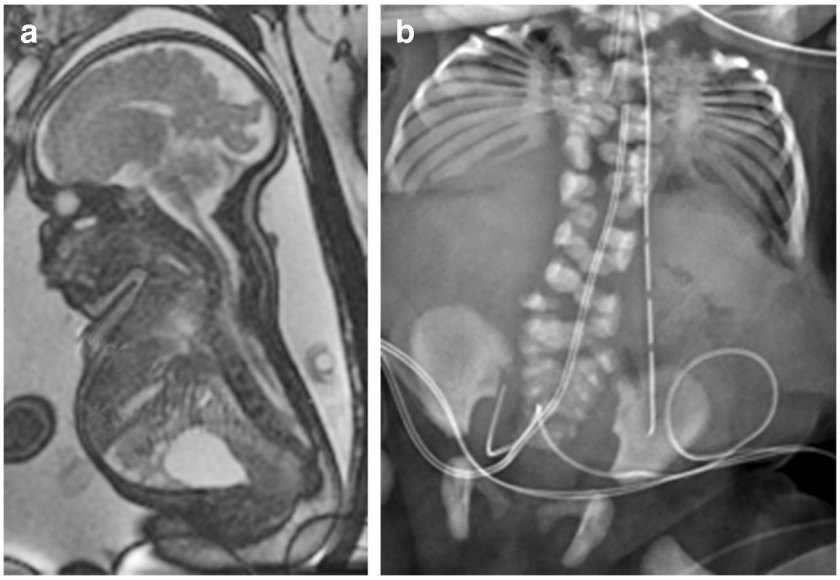

Fig. 13 Spondylothoracic dysostosis in a 33-week female fetus. **a** Sagittal single-shot fast spin-echo (SSFSE) MR image demonstrates foreshortening of the chest and spine with increased anteroposterior distance of the thorax. After thorough investigation, the ribs were poorly evaluated and the suspected vertebral anomalies could not be adequately depicted. **b** Anteroposterior postnatal radiograph of the chest and abdomen obtained at 1 day old demonstrates innumerable vertebral anomalies throughout the spine, including multiple fusion anomalies of the posterior ribs with crablike deformity of the rib cage, in keeping with spondylothoracic dysostosis

of gestational age [29]. The first visible secondary ossification center is the calcaneus, appearing at the end of the 23rd week of gestation by US. By 25 weeks, the talus ossification center appears. The distal femoral epiphyseal ossification becomes visible by 33 weeks of gestation and the proximal tibial ossification at 36 weeks [30]. Data regarding the appearance of ossification centers depicted by MR are limited. In a small population, Nemec et al. [31] demonstrated that on EPI, the distal femoral secondary ossification center can be reliably seen by 35 weeks and as early as 25 weeks 3 days of gestation.

Upper extremities

The upper limb bud forms on approximately Day 26 of gestation and develops in a proximo-distal fashion. By the end of the eighth week of gestation, the entire upper limb is formed and contains all anatomical structures such as cartilage, joints and soft tissue. The hand develops from apoptosis of the fetal hand paddle, in a distal-to-proximal orientation. Metacarpals are ossified by 12–16 weeks. This process is regulated by numerous molecular interactions, and when failure of a specific pathway occurs, an upper limb deficiency results [32].

Approximately 10–20% of all congenital malformations have upper limb elements [33]. The spectrum of upper limb anomalies varies from subtle finger deformities to complete absence of limbs and can be isolated or associated with a chromosomal disorder (Fig. 14) (Table 4) [33]. Malformations of the hands are classified by the predominant anomaly: abnormal alignment (i.e. clenched hand), thumb anomalies, abnormal calcifications or abnormal number of components (i.e. polydactyly or ectrodactyly) (Fig. 15). Epidemiological studies have shown that preaxial anomalies (absence or partial absence of thumb, first metacarpal or radius; or hallux, first metatarsal, or tibia) are more likely to be shared with anomalies in other organ systems such as the heart, urinary tract and gastrointestinal tract. In contrast, transverse defects (absence of distal structures — metacarpals or phalanges — of the limbs) tend to be seen with craniofacial anomalies such as facial clefts and micrognathia that can be linked to disruptive events in early pregnancy [34]. In a series by Nemec et al. [3], the visualization of upper extremity abnormalities on fetal US was not only confirmed by MR, but in almost half of cases where MR and US findings were compared, MR added information, especially in regard to fetal neuroimaging.

Lower extremities

The lower limb begins to develop approximately 2 days after the upper limb starts to form. The molecular factors that control limb development in both upper and lower limbs are similar, and thus symmetrical abnormalities of the arms and legs are not uncommon [35]. The long bones of the legs ossify by 8 weeks of gestation and metatarsals by 12–16 weeks. Two lower-extremity deformities that might be markers for multisystem anomalies are talipes equinovarus (clubfoot) and congenital vertical talus (rocker-bottom foot). When either anomaly is detected prenatally, a thorough search for additional anomalies should be performed, particularly within the brain and spine.

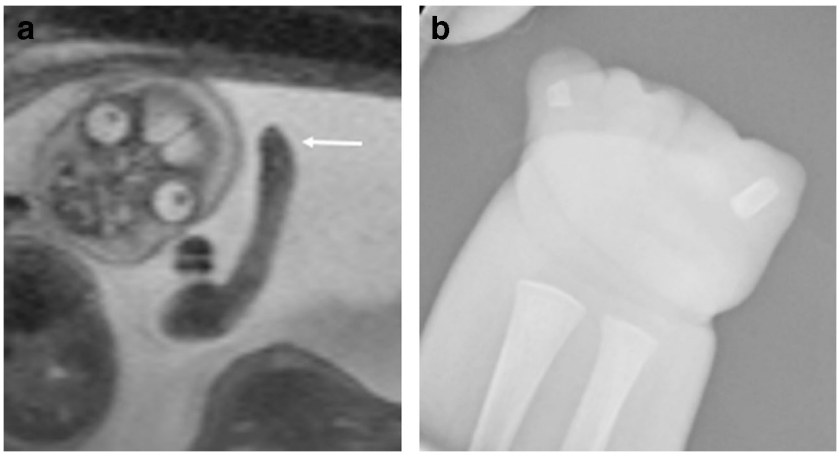

Fig. 14 Congenital hand deformity in a 23-week male fetus. **a** Coronal single-shot fast spin-echo MR image demonstrates a foreshortened appearance of the left hand with no identifiable digits (*arrow*). **b** Postnatal anteroposterior radiograph obtained shortly after birth shows terminal transverse limb reduction defect with truncation of the hand at the level of the proximal metacarpals, with complete adactylia. Other anomalies were present but not a unifying diagnosis

Table 4 Summary of specific congenital defects that are associated with upper limb differences [33]

Pathology	Upper limb difference	Associated malformations
VACTERL association	Radial longitudinal deficiency	Vertebral abnormalities, anal atresia, cardiac abnormalities, trachea-esophageal fistula, esophageal atresia, renal defects, lower limb anomalies
TAR syndrome	Radial longitudinal deficiency	Thrombocytopenia, cardiac defects
Fanconi anemia	Radial longitudinal deficiency, absent thumb	Thrombocytopenia, high diepoxybutane-induced chromosomal breakage in fetal cells
Ulnar–mammary syndrome	Ulnar ray defects (hypoplastic or absent ulna with 3rd, 4th, 5th digits, camptodactyly, hypoplastic terminal phalanx)	Apocrine gland abnormalities, hypogenitalism
Holt–Oram syndrome	Triphalangeal thumb, radial longitudinal deficiency, polydactyly	Cardiac defects
Brachmann–de Lange syndrome	Upper limb malformation	Diaphragmatic hernia, IUGR, facial anomalies
Aese syndrome	Triphalangeal thumb, radial longitudinal deficiency	Anemia, cardiac defects
FADS	Clenched hands, camptodactyly	Arthrogryposis, clubfeet, IUGR, craniofacial dysmorphism, polyhydramnios, lung hypoplasia
Rubinstein–Taybi syndrome	Broad radially deviated thumbs	Large abducted toes, abnormal facies, cerebellar hypoplasia
Poland syndrome	Unilateral upper limb hypoplasia, syndactyly	Ipsilateral rib cage hypoplasia
Apert syndrome	Syndactyly, mitten hand	Craniosynostosis
Carpenter syndrome	Syndactyly, brachydactyly, polydactyly	Craniosynostosis, acrocephaly
Pfeiffer syndrome	Syndactyly, brachydactyly, broad thumbs	Craniosynostosis
Osteochondral dysplasia	Trident hand	IUGR
Diastrophic dysplasia	Hitchhiker thumb	IUGR
Nail–patella syndrome	Nail abnormalities (agenesis, hypoplasia, splitting, pitting, triangular lunulae), cubitus valgus	Patella abnormalities (agenesis, hypoplasia, dysplasia, dislocation)
Oral–facial digital syndrome	Fingers and toes syndactyly, brachydactyly, clinodactyly, polydactyly	Oral (split tongue, cleft palate, hyperplastic frenula) and facial (cleft lip, flat nasal bridge, hypertelorism)
Weaver syndrome	Camptodactyly, joint contractures	Overgrowth, macrocephaly, broach forehead, hypertelorism, low-set ears, kyphoscoliosis
Trisomy 13	Camptodactyly, polydactyly	IUGR, neural and cardiac defects
Trisomy 18	Clenched hand, camptodactyly	IUGR, craniofacial dysmorphism, cardiac defects
Trisomy 21	Clinodactyly	Increased nuchal translucency, cardiac defects, nasal bone hypoplasia

FADS fetal akinesia deformation sequence, *IUGR* intrauterine growth restriction, *TAR* thrombocytopenia with absent radius, *VACTERL* vertebral, anal and cardiac anomalies, tracheoesophageal fistula, and renal and limb malformations

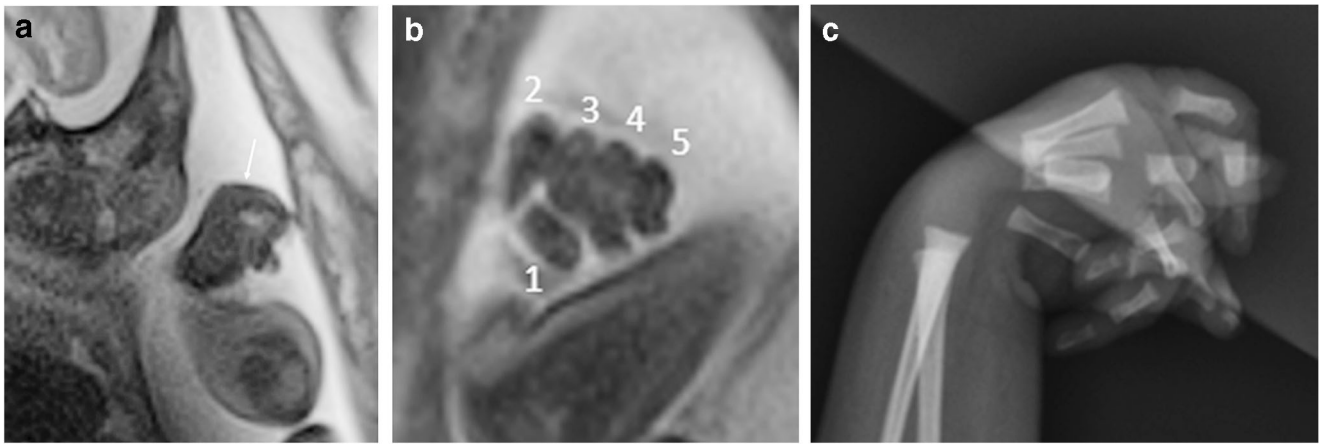

Fig. 15 Clenched fist in a 32-week male fetus. **a**, **b** Sagittal and coronal single-shot fast spin-echo MR images show the hand is clenched (*arrow* in **a**). Discrete fingers are depicted (*numbers 1–5* in **b**). **c** Postnatal lateral radiograph of the hand at Day 1 after birth demonstrates abnormal flexed, clenched appearance of the digits

Talipes equinovarus

Talipes equinovarus is a common congenital structural abnormality of the lower leg in which the forefoot and the heel are inverted, giving rise to a club-like appearance. There is subluxation of the talo-calcaneo-navicular joint with underdevelopment of the soft tissues of the foot and frequently the calf and peroneal muscles. Approximately 50% are bilateral and there is a male predominance [36]. Talipes equinovarus might be associated with myelodysplasia, arthrogryposis or multiple congenital abnormalities, but it is most commonly an idiopathic, isolated birth defect. The prevalence of additional congenital anomalies or chromosomal abnormalities in patients with clubfoot varies across studies, ranging 24–50% [37].

Sagittal imaging of the normal lower leg shows the foot perpendicular to the shafts of the tibia and fibula; however, in talipes equinovarus there is a fixed deformity of the forefoot in adduction and pronation toward the hindfoot (Fig. 16). This configuration should be seen throughout the course of the study [38]. Use of dynamic imaging might be useful to distinguish a fixed from a flexible/positional foot deformity [39]. Servaes et al. [38] demonstrated that correlation of MRI with US in the evaluation of talipes equinovarus yielded a sensitivity of 100% and specificity of 85%. The authors also demonstrated that the plane of imaging with respect to the foot rather than the particular sequence used (SSFSE or EPI) was more useful for depiction. In another study comparing MRI and US in the evaluation of talipes equinovarus, MRI confirmed the US diagnosis, clarified questionable US results, and added findings with special attention to the central nervous system in fetuses with complex talipes equinovarus [39]. Additional MR findings were seen in almost one-fifth of the cases, predominately related to spine and brain anomalies (Fig. 17). It is important to search for clubfoot on fetal MR studies designed to evaluate deformities of the spine or other congenital anomalies.

Congenital vertical talus

Congenital vertical talus (rocker-bottom flatfoot) is a rare rigid flatfoot disorder with hindfoot valgus and equinus with midfoot dorsiflexion and forefoot abduction. It is caused by a fixed dorsal dislocation of the navicular on the head of the talus. Approximately one-half of cases of congenital vertical talus occur in conjunction with neurologic disorders or known genetic defects/syndromes; the other cases are idiopathic [40]. The most common neurologic disorders associated with congenital vertical talus are distal arthrogryposis and myelomeningocele. It is also seen in aneuploidy (Chromosomes 13, 15 and 18); a variety

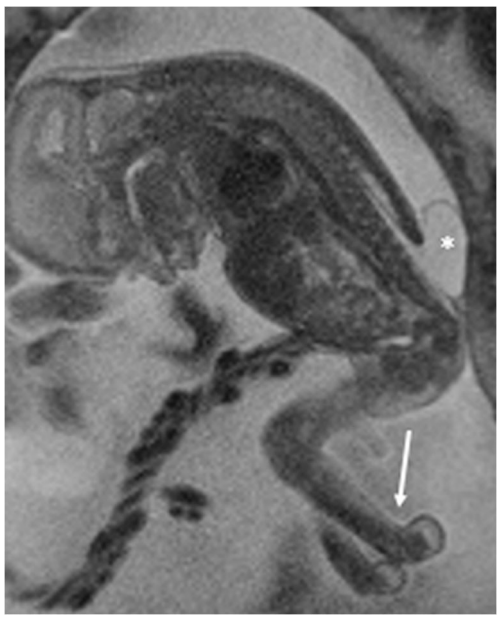

Fig. 16 Myelomeningocele and bilateral clubfeet in a 22-week male fetus. Sagittal single-shot fast spin-echo MR image demonstrates abnormal configuration of both feet with respect to the tibiae (*arrow*), fixed throughout the study. Lumbosacral myelomenigocele is present (*asterisk*)

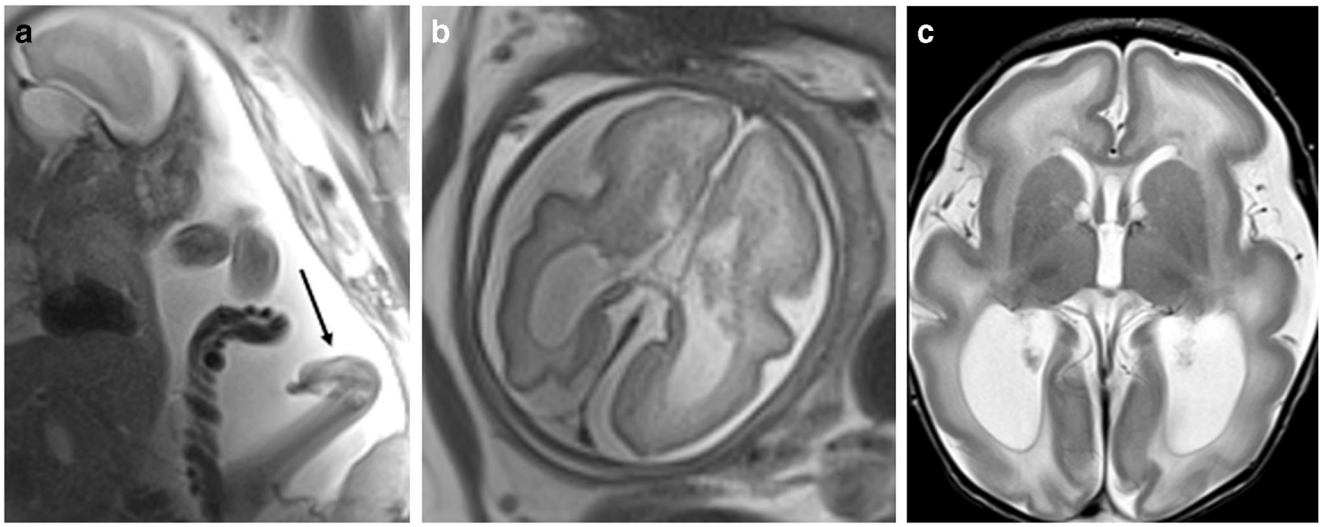

Fig. 17 Clubfoot and brain abnormalities in a 32-week male fetus. Clubfoot was seen on US and MRI was ordered to evaluate for additional anomalies. **a** Sagittal single-shot fast spin-echo (SSFSE) MR image of the body demonstrates clubfoot deformity (*arrow*). **b** Axial SSFSE of the brain shows decreased sulcation for gestational age, suggestive of malformation of cortical development with ventriculomegaly. **c** Postnatal axial T2-weighted image obtained at Day 1 of age shows lissencephaly with smooth cortex and simplified gyration with ventriculomegaly

of syndromes including spinal muscular atrophy, neurofibromatosis, Marfan, De Barsy, Costello and Rasmussen; and split foot limb malformation disorders [40, 41].

On prenatal imaging, differentiating congenital vertical talus from talipes equinovarus can be challenging. On MRI, congenital vertical talus is best depicted on sagittal imaging, seen as a protuberant heel, convex plantar surface and distal foot dorsiflexion (Fig. 18) [41]. Partial or oblique images might lead to erroneous characterization or misdiagnosis of clubfoot. Rubio et al. [41] demonstrated that US is superior to MRI in imaging the fetal foot, given the ability to maneuver the US probe in the plane of the foot in real time. MRI, however, was useful to confirm diagnosis, particularly in cases of larger maternal body habitus or difficult fetal lie [41]. In their case study of 24 fetuses, there were no isolated cases of congenital vertical talus; fetal MRI was a useful adjunct in further delineating additional anomalies in the brain, spine, face, abdominal wall, heart and other limbs [41].

Muscles and fetal movement

In the third trimester, normal individual muscles might not be differentiated from the underlying bones on SSFSE sequences. However, EPI creates nice distinction of the muscle and bone within the extremities. MRI can be useful to demonstrate abnormal contours or muscle thickness as well as atrophy. Increased T1-weighted and T2-weighted signal intensity might indicate muscular edema or fatty transformation [1]. Abnormal muscular development might be associated with limb abnormalities such as arthrogryposis, spinal muscle dystrophy or muscle dystrophy (Fig. 19) [11].

Fetal movement can be a significant indicator of fetal health. Studies show that decreased fetal movement might precede fetal demise/stillbirths [42]. Physical fetal movements are a normal part of musculoskeletal development. When movement of the fetus in the uterus is limited, such as in neuromuscular disorders, it can lead to abnormal joint

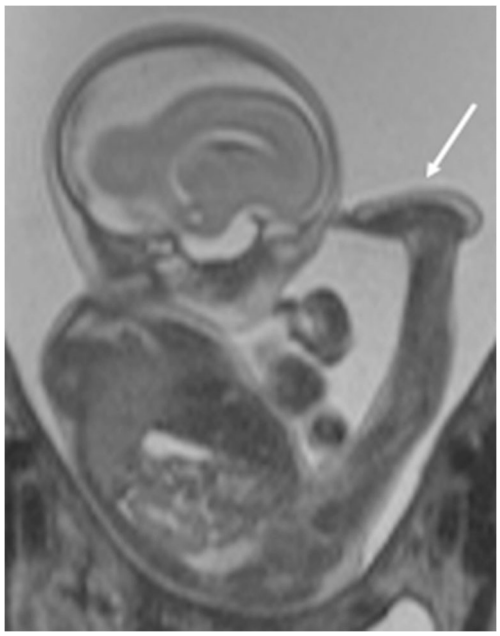

Fig. 18 Rocker-bottom flatfoot in a 21-week male fetus. Sagittal single-shot fast spin-echo MR image of the fetus demonstrates hyperflexed hip and extended knee, which were unchanged in position throughout the examination. There is a rocker-bottom configuration of the foot with a protuberant heel, convex plantar surface and distal foot dorsiflexion (*arrow*). Other anomalies included omphalocele, cystic hygroma and spine anomalies (not depicted)

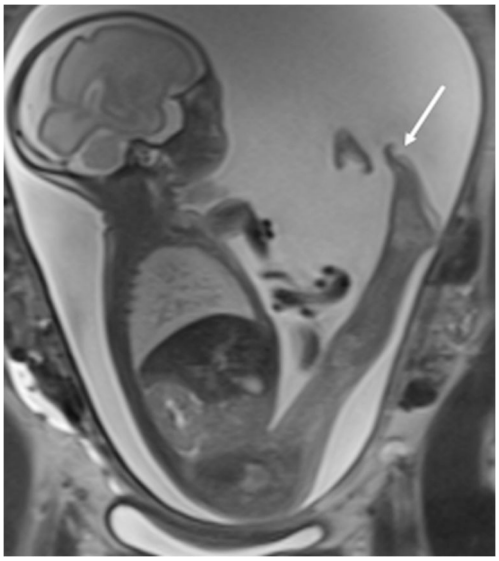

Fig. 19 Arthrogryposis in a 26-week female fetus. Sagittal single-shot fast spin-echo MR image of the fetus shows abnormal joint and muscular development of the legs, which are decreased in bulk. The leg remained with hip in flexion and knee in extension with the toes pointed (*arrow*). There was absence of lower limb movement throughout the duration of the study. Postnatally, all extremities were abnormal, with flexion deformities of the shoulders and wrists

development (Fig. 20) [43]. Cine imaging adds information regarding neurologic function and can serve as a prognostic indicator. For example, cine imaging of a fetus with a lumbar myelomeningocele might show lack of movement in extended deformed legs with clubfeet, suggestive of severe nerve impairment [44].

Amniotic band syndrome

Amniotic band syndrome comprises a wide spectrum of abnormalities in which fetal parts become entrapped by a disrupted amnion. While the etiology is unknown, it is theorized that early disruption of the amnion allows the embryo or fetus to enter the chorionic cavity and contact the chorionic side of the amnion, leading to fibrous bands that can compromise fetal body components. Alternatively, amniotic bands might be caused by vascular insults. The hands and feet are involved in 80% of cases. Umbilical cord constriction by amniotic bands occurs in approximately 10% of cases, and rarely the trunk or head is involved. Limb anomalies can result, including amputation, acrosyndactyly, oligodactyly, talipes equinovarus or simply soft-tissue constriction. Other associated abnormalities include cleft lip and palate, craniofacial disruptions, neural tube defects, cranial defects, scoliosis and body wall defects [2].

Magnetic resonance imaging plays a complementary role to US in evaluating the effects of amniotic band syndrome. On MRI, amniotic bands appear as low T2 signal linear strands. When a limb is involved, the band causes focal constriction of the soft tissues with or without edema, which appears as increased soft-tissue thickness and fluid signal intensity of the distal aspect of the affected extremity (Fig. 21) [2]. Typically, associated decreased motion of the affected limb is evident on dynamic imaging, with variable levels of limb amputation, limb constriction or atrophy [2]. Neuman et al. [2] determined that amniotic bands are best seen on balanced steady-state

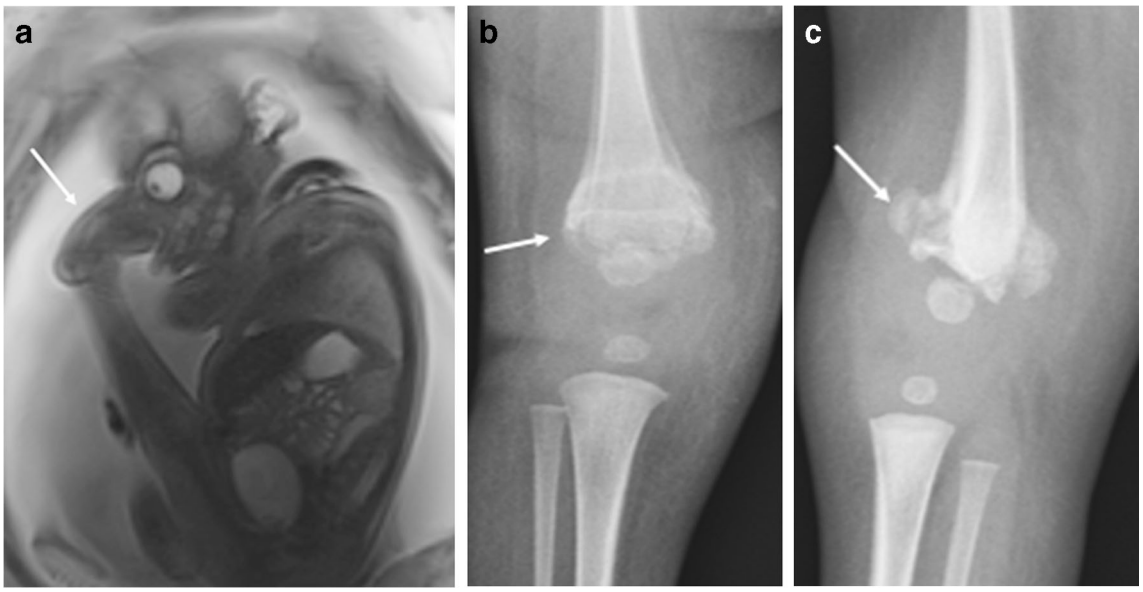

Fig. 20 Arthrogryposis and clubfoot in a 32-week male fetus. **a** Sagittal single-shot fast spin-echo MR image of the fetus demonstrates hip flexion and knee extension, which remained throughout the examination with limited motion and clubfoot deformity (*arrow*). **b**, **c** Anteroposterior and lateral radiographs of the knee obtained at Day 10 of age demonstrate genu recurvatum with a healing distal femoral metaphyseal fracture (*arrows*). Abundant callous formation is present, suggesting the fracture was sustained in utero

gradient echo sequences, likely because of the inherent contrast resolution. When an extremity is involved, Doppler US remains the imaging modality for assessing blood flow in the distal aspect of the limb. If distal flow is absent, the limb might not be salvageable and fetoscopic band release might not be performed. If flow is decreased but present, surgical intervention might be considered because fetoscopic release of amniotic bands has been shown to potentially improve perfusion to salvage growth of the affected extremities [10].

Skeletal dysplasias

Skeletal dysplasias (or osteochondrodysplasias and dysostoses) represent a large, heterogeneous group of conditions with various abnormalities of the skeleton. By definition, the osteochondrodysplasias refer to generalized abnormalities of the skeleton, whereas the dysostoses are a group of disorders that have a single or group of abnormal bones. However, as more is learned about these disorders, the distinction is blurred [45]. They encompass more than 400 specific diagnoses, for which associated mutations in more than 300 genes have been identified. Although the occurrence of each individual skeletal dysplasia might be rare, collectively they account for a significant number of newborns with congenital anomalies [45].

Skeletal dysplasias are often detected by routine prenatal US at about 20 weeks of gestation. A main utility of US is determining whether the skeletal dysplasia is potentially lethal. Lethality is predominately from pulmonary hypoplasia and inability to achieve adequate ventilation in the immediate neonatal period, which can be estimated on US with biometric ratios [27, 46]. Prenatal US has an estimated accuracy of 40–80% in diagnosing skeletal dysplasias [47, 48]. Ultrasound, however, has limitations because of the low incidence, multitude of possible diagnoses, overlapping features and phenotypic variability. In addition, some dysplasias are not detected until the late third trimester and technical factors such as maternal body habitus, oligohydramnios and sonographer expertise can affect evaluation. MRI has proved to be a useful adjunct tool for detecting skeletal dysplasia, providing supplemental information about skeletal anomalies when the screening US is abnormal [24, 47–49]. Imaging of the thorax is based on the observed/expected (O/E) lung volume, which is predictive of lethality in skeletal dysplasias. An O/E less than 48% is predictive of lethality [49]. In a recent study by Gilligan et al. [47], the addition of fetal MRI in the prenatal evaluation was shown to be useful in not only providing lung volumes, but also adding information regarding findings in the brain, calvarium and cartilage.

Skeletal dysplasias manifest with one or more bone findings including abnormal length, shape, number or density

Table 5 Imaging approach to the skeletal dysplasias adapted from [48]

Reference skeletal structures	MRI assessment
Fetal skull	Frontal bossing
	Macrocephaly
	Micrognathia
	Cleft palate
	Hyper−/hypotelorism
Thorax	Chest biometry, O/E
	Overall morphology
	Rib anomalies
	Scapulae
	Clavicles; overall shape and size
Spine	Abnormal curvature
	Fractures
	Platyspondyly
Pelvis	Size
	Overall shape
Long bones	Abnormal curvature
	Fractures
	Hypoplasia, absence, malformation
	Intersegmentary comparison — rhizomelia, mesomelia, acromelia, severe micromelia
Hands and feet	Fingers — size, polydactyly, syndactyly, clinodactyly, abnormal position
Fetal movement	Hypokinesia

O/E observed/expected

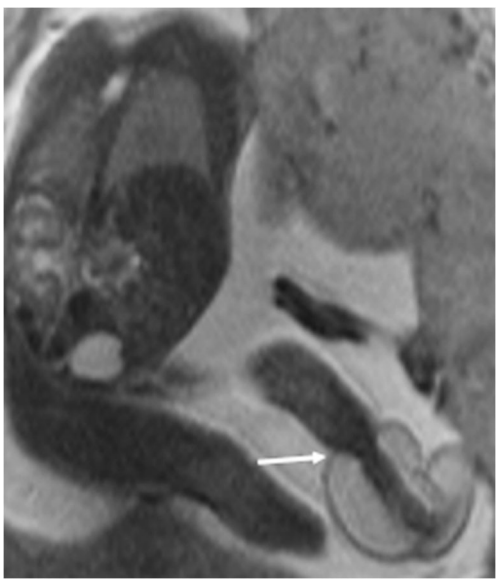

Fig. 21 Amniotic band in a 22-week fetus. Sagittal single-shot fast spin-echo MR image of the fetus shows focal soft-tissue constriction of the lower extremity (*arrow*), with extensive distal soft-tissue edema depicted by increased thickness and fluid signal. The osseous structures of the distal leg and foot were poorly delineated

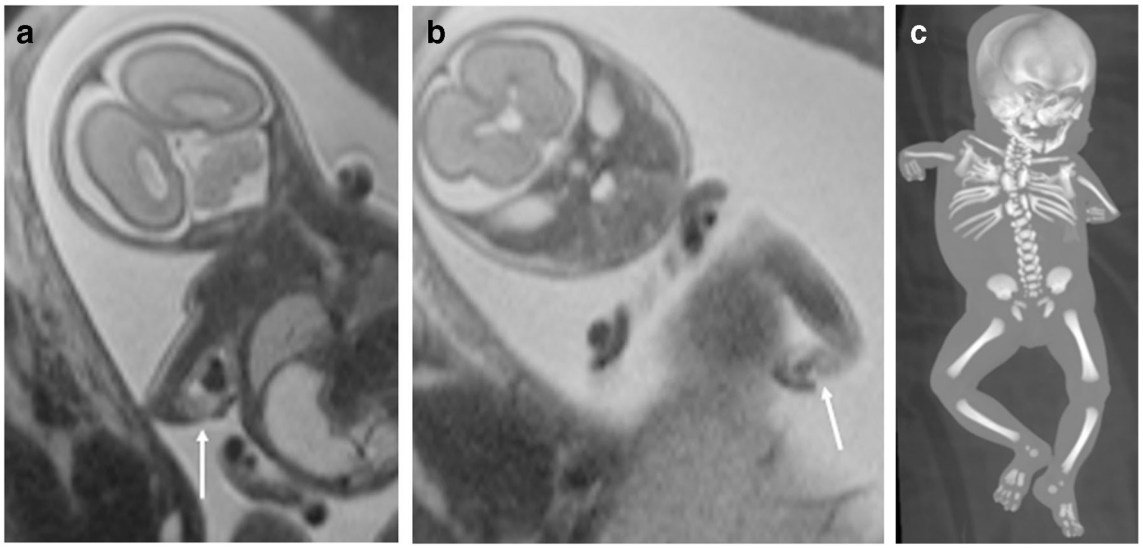

Fig. 22 Spine and upper limb anomalies in a 24-week female fetus. **a, b** Coronal single-shot fast spin-echo MR images of the fetus demonstrate poor delineation of the bony anomalies of the thoracic cage and spine. Both the right (**a**) and left (**b**) arms are abnormally foreshortened, with radial and ulnar aplasia and malformed hands (*arrows*). The thorax is small. **c** Coronal reformatted low-dose fetal CT better depicts the numerous skeletal anomalies of the thorax, spine and upper limbs. There was subsequent fetal demise in this case

[47]. A standard approach to evaluating skeletal dysplasias on MRI is presented in Table 5 [48]. It should be noted that bone density is not optimally assessed on MR images and US is preferred for evaluating demineralization. In addition, although MR is useful in the brain and calvarium, in our experience MR might not offer additional information on the bones in complex skeletal dysplasias involving the thorax and spine. An important advance in the field of prenatal imaging of dysplasias is low-dose fetal CT. Low-dose fetal CT affords exquisite depiction of the fetal bones, allows accurate assessment of bone mineralization and has been shown to dramatically improve diagnosis in complex skeletal anomalies (Fig. 22) [28]. More recent protocol modifications have allowed for marked decrease in radiation dose. In the appropriate clinical setting, ultra-low-dose CT can add vital information that assists in prenatal counseling and postnatal care of the child [46].

Conclusion

Magnetic resonance imaging is an emerging modality to evaluate the fetal musculoskeletal system. Steady-state T2-weighted images and EPI sequences can be used to evaluate ossified bone length and morphology while thick-slab 3-D imaging allows for an overall assessment of fetal skeletal morphology. Dynamic MR aids in the depiction of distal limb abnormalities, fetal motion disorders and contractions. As an adjunct to US, MRI can assist in management and offer a more complete assessment for prognostication.

Compliance with ethical standards

Conflicts of interest None

References

1. Nemec SF, Nemec U, Brugger PC et al (2012) MR imaging of the fetal musculoskeletal system. Prenat Diagn 32:205–213
2. Neuman J, Calvo-Garcia MA, Kline-Fath BM et al (2012) Prenatal imaging of amniotic band sequence: utility and role of fetal MRI as an adjunct to prenatal US. Pediatr Radiol 42:544–551
3. Nemec SF, Kasprian G, Brugger PC et al (2011) Abnormalities of the upper extremities on fetal magnetic resonance imaging. Ultrasound Obstet Gynecol 38:559–567
4. Laor T, Jaramillo D (2009) MR imaging insights into skeletal maturation: what is normal? Radiology 250:28–38
5. Nemec SF, Nemec U, Brugger PC et al (2011) Skeletal development on fetal magnetic resonance imaging. Top Magn Reson Imaging 22:101–106
6. Kovacs CS (2011) Bone development in the fetus and neonate: role of the calciotropic hormones. Curr Osteoporos Rep 9:274–283
7. Laor T, Jaramillo D (2020) It's time to recognize the perichondrium. Pediatr Radiol 50:153–160
8. Schumacher R, Seaver LH, Spranger J (2010) Fetal radiology a diagnostic atlas, 2nd edn. Springer-Verlag, Heidelberg
9. Victoria T, Johnson AM, Edgar JC et al (2016) Comparison between 1.5-T and 3-T MRI for fetal imaging: is there an advantage to imaging with a higher field strength? AJR Am J Roentgenol 206:195–201
10. Lyons K, Cassady C, Mehollin-Ray A, Krishnamurthy R (2015) Current role of fetal magnetic resonance imaging in body anomalies. Semin Ultrasound CT MR 36:310–323
11. Nemec U, Nemec SF, Krakow D et al (2011) The skeleton and musculature on foetal MRI. Insights Imag 2:309–318
12. Patel MD, Swinford AE, Filly RA (1994) Anatomic and sonographic features of the fetal skull. J Ultrasound Med 13:251–257

13. Rubio EI, Blask A, Bulas DI (2016) Ultrasound and MR imaging findings in prenatal diagnosis of craniosynostosis syndromes. Pediatr Radiol 46:709–718
14. Ketwaroo PD, Robson CD, Estroff JA (2015) Prenatal imaging of craniosynostosis syndromes. Semin Ultrasound CT MR 36:453–464
15. Werner H, Castro P, Daltro P et al (2018) Prenatal diagnosis of Apert syndrome using ultrasound, magnetic resonance imaging, and three-dimensional virtual/physical models: three case series and literature review. Childs Nerv Syst 34:1563–1571
16. Giancotti A, D'Ambrosio V, De Filippis A et al (2014) Comparison of ultrasound and magnetic resonance imaging in the prenatal diagnosis of Apert syndrome: report of a case. Childs Nerv Syst 30: 1445–1448
17. Mailath-Pokorny M, Klein K, Worda C et al (2012) Maxillary dental arch biometry: assessment with fetal MR imaging. Prenat Diagn 32:530–535
18. Nemec U, Nemec SF, Brugger PC et al (2015) Normal mandibular growth and diagnosis of micrognathia at prenatal MRI. Prenat Diagn 35:108–116
19. Wang G, Shan R, Zhao L et al (2011) Fetal cleft lip with and without cleft palate: comparison between MR imaging and US for prenatal diagnosis. Eur J Radiol 79:437–442
20. Resnick CM, Estroff JA, Kooiman TD et al (2018) Pathogenesis of cleft palate in Robin sequence: observations from prenatal magnetic resonance imaging. J Oral Maxillofac Surg 76:1058–1064
21. Rogers-Vizena CR, Mulliken JB, Daniels KM, Estroff JA (2016) Prenatal features predictive of Robin sequence identified by fetal magnetic resonance imaging. Plast Reconstr Surg 137:999e–1006e
22. Antonakopoulos N, Bhide A (2019) Focus on prenatal detection of micrognathia. J Fetal Med 6:107–112
23. Upasani VV, Ketwaroo PD, Estroff JA et al (2016) Prenatal diagnosis and assessment of congenital spinal anomalies: review for prenatal counseling. World J Orthop 7:406–417
24. Yazici Z, Kline-Fath BM, Laor T, Tinkle BT (2010) Fetal MR imaging of Kniest dysplasia. Pediatr Radiol 40:348–352
25. Shekdar K (2016) MRI of fetal spine and extremities. In: Masselli G (ed) MRI of fetal and maternal diseases in pregnancy. Springer International Publishing, Switzerland, pp 139–158
26. Mekonen HK, Hikspoors JP, Mommen G et al (2015) Development of the ventral body wall in the human embryo. J Anat 227:673–685
27. Dighe M, Fligner C, Cheng E et al (2008) Fetal skeletal dysplasia: an approach to diagnosis with illustrative cases. Radiographics 28: 1061–1077
28. Victoria T, Epelman M, Coleman BG et al (2013) Low-dose fetal CT in the prenatal evaluation of skeletal dysplasias and other severe skeletal abnormalities. AJR Am J Roentgenol 200:989–1000
29. Donne HD Jr, Faundes A, Tristao EG et al (2005) Sonographic identification and measurement of the epiphyseal ossification centers as markers of fetal gestational age. J Clin Ultrasound 33:394–400
30. Gentili P, Trasimeni A, Giorlandino C (1984) Fetal ossification centers as predictors of gestational age in normal and abnormal pregnancies. J Ultrasound Med 3:193–197
31. Nemec U, Nemec SF, Weber M et al (2013) Human long bone development in vivo: analysis of the distal femoral epimetaphysis on MR images of fetuses. Radiology 267:570–580
32. Al-Qattan MM, Yang Y, Kozin SH (2009) Embryology of the upper limb. J Hand Surg Am 34:1340–1350
33. Alrabai HM, Farr A, Bettelheim D et al (2017) Prenatal diagnosis of congenital upper limb differences: a current concept review. J Matern Fetal Neonatal Med 30:2557–2563
34. Rosano A, Botto LD, Olney RS et al (2000) Limb defects associated with major congenital anomalies: clinical and epidemiological study from the International Clearinghouse for Birth Defects Monitoring Systems. Am J Med Genet 93:110–116
35. Sifakis S, Basel D, Ianakiev P et al (2001) Distal limb malformations: underlying mechanisms and clinical associations. Clin Genet 60: 165–172
36. Barry M (2005) Prenatal assessment of foot deformity. Early Hum Dev 81:793–796
37. Dobbs MB, Gurnett CA (2009) Update on clubfoot: etiology and treatment. Clin Orthop Relat Res 467:1146–1153
38. Servaes S, Hernandez A, Gonzalez L et al (2010) Fetal MRI of clubfoot associated with myelomeningocele. Pediatr Radiol 40: 1874–1879
39. Nemec U, Nemec SF, Kasprian G et al (2012) Clubfeet and associated abnormalities on fetal magnetic resonance imaging. Prenat Diagn 32:822–828
40. Miller M, Dobbs MB (2015) Congenital vertical talus: etiology and management. J Am Acad Orthop Surg 23:604–611
41. Rubio EI, Mehta N, Blask AR, Bulas DI (2017) Prenatal congenital vertical talus (rocker bottom foot): a marker for multisystem anomalies. Pediatr Radiol 47:1793–1799
42. Efkarpidis S, Alexopoulos E, Kean L et al (2004) Case-control study of factors associated with intrauterine fetal deaths. MedGenMed 6:53
43. Verbruggen SW, Loo JH, Hayat TT et al (2016) Modeling the biomechanics of fetal movements. Biomech Model Mechanobiol 15:995–1004
44. Guo WY, Ono S, Oi S et al (2006) Dynamic motion analysis of fetuses with central nervous system disorders by cine magnetic resonance imaging using fast imaging employing steady-state acquisition and parallel imaging: a preliminary result. J Neurosurg 105:94–100
45. Krakow D, Lachman RS, Rimoin DL (2009) Guidelines for the prenatal diagnosis of fetal skeletal dysplasias. Genet Med 11:127–133
46. Victoria T, Zhu X, Lachman R et al (2018) What is new in prenatal skeletal dysplasias? AJR Am J Roentgenol 210:1022–1033
47. Gilligan LA, Calvo-Garcia MA, Weaver KN, Kline-Fath BM (2020) Fetal magnetic resonance imaging of skeletal dysplasias. Pediatr Radiol 50:224–233
48. Berceanu C, Gheonea IA, Vladareanu S et al (2017) Ultrasound and MRI comprehensive approach in prenatal diagnosis of fetal osteochondrodysplasias. Cases series. Med Ultrason 19:66–72
49. Weaver KN, Johnson J, Kline-Fath B et al (2014) Predictive value of fetal lung volume in prenatally diagnosed skeletal dysplasia. Prenat Diagn 34:1326–1331